Exergy Performance of a Natural Circulation Solar Collector System Using Aluminum Oxide, Copper, and Copper Oxide Nanofluids

Norouzi, Nima

Department of Energy Engineering and Physics, Amirkabir University of Technology (Tehran Polytechnic), Tehran, I.R. IRAN

Bozorgian, Alireza*[+]

Department of Chemical Engineering, Mahshahr Branch, Islamic Azad University, Mahshahr, I.R. IRAN

ABSTRACT: *Most of the global energy demand is related to the residential and commercial sectors. This significant share in the energy demand portfolio also shows a significant share of greenhouse gas emissions from the great cities. This is why renewable and other cleaner energy sources have been attractive in the last three decades. Solar collectors, energy storage, and photovoltaic cells are the most suitable clean technologies applicable to generate and store electricity, cooling, and heating demand in the residential sector. Due to this increasing attractiveness, much research has been done on those technologies to increase the systems' efficiency. One of the most important methods to improve these systems' performance can directly improve thermal conductivity and heat transfer. In this study, the collector is modeled in the system's fluent software and the main parameters are estimated for different nanoparticles. Then an exergy analysis is done to find the entropy generation and exergy destruction of the system to detect the main sources of the irreversibility in the system. Also, the effect of different parameters is studied on the exergy efficiency of this system. The results show that the value of temperature generation in cold climates has been higher than in hot climates, and increasing the inflow and collecting water level has increased consumer water Temperature. Using copper nanofluids increases solar water heaters' efficiency by up to 67%, while aluminum oxide and copper oxide nanofluids have 74% and 47% efficiency, respectively.*

KEYWORDS: Nanoparticles, Exergy analysis, Solar thermal, natural draft.

INTRODUCTION

In Indirect (or volumetric) collectors, light is absorbed by volume, while other collectors, such as flat-panel collectors, absorb sunlight by the surface, which raises the surface Temperature and, consequently, increases heat loss on the surface. The outdoor environment leads through the surface [1]. Under the same conditions, the solar collector shows direct absorption (volumetric) due to the removal of pipes, also shows less heat resistance against

*** To whom correspondence should be addressed.*
+ E-mail: alireza.bozorgian@iau.ac.ir
1021-9986/2023/3/989-1005 17/$/6.07

the conversion of sunlight into useful heat [2]. The sun, which receives energy through particle-filled liquids (liquid-particle suspensions), has been analyzed by various researchers using theoretical and experimental methods. One of the first direct absorption collectors using a liquid-working fluid was a collector, which was tested using a black fluid (Indian ink-water) to absorb radiation directly and improve efficiency in the late 1970s [3]. This black fluid was a solution of black particles with micron-sized aggregates in transparent, spiral, flowing, and exposed to sunlight plastic tubes and *Chang* stated in his research that due to the removal of metal from the collector building and glass and plastic and reducing costs, corrosion problems would also be eliminated [3]. In recent years, researchers have studied the effect of using nanofluid (liquid-nanoparticle suspension) as a working fluid on improving the efficiency of direct absorption solar collectors compared to flat-panel collectors (Sharpen). As the first research, *Tiagi et al.* [4] Examined aluminum in water numerically and concluded that under similar operating conditions, a 10% increase in efficiency is achieved by using a new collector compared to a conventional flat plate solar collector. The first experimental study on solar collectors for direct absorption of nanosilbyanes was conducted by *Ethanikar et al.* Using graphite nanoparticles, carbon and silver nanotubes were confirmed compared to conventional collectors. He co-authored Golden with another study on the economic use of nanofluids in solar collectors. According to their results, solar collectors containing nanofluids have higher thermal efficiency and less compensatory energy than conventional collectors [6]. The results of research conducted by *Atanikar et al.* [7] on the effect of nanoparticle size on thermal performance showed that the smaller the particle diameter, the higher the collector efficiency.

Virarajavan et al. [8] presented an analytical model for the design of solar volumetric collectors. They investigated the base fluid of the 1-VP terminal with graphite nanoparticles in a channel one centimeter deep and concluded that the system efficiency was about 35% during the 0.86 dimensionless comes.

Lajevardi et al. [9] numerically investigated the application of graphite nanofluids to absorb solar radiation. Their results showed that graphite nanofluid with a volume component of 0.000025% absorbs more than 50% of the input radiation; While, only $ 0.0045 per liter increases the cost.

All thermodynamic processes involve irreversibility that reduces system performance. The amount of this irreversibility is determined by the entropy production rate. Heat transfer and entropy production indirect absorption solar collector containing copper-water nanofluid has been investigated by *Parvin et al.* [10]. Their study focused on the effect of the nanoparticle volume component and Reynolds number on the Nusselt number, entropy production, and collector efficiency. The results showed that increasing the volumetric component and Reynolds number, Nusselt number, and entropy production increases.

Gupta et al. [11] conducted an experimental study of direct absorption solar collectors. The experiment was performed using four different volume fractions, with Al2O3 nanoparticles measuring 20 nm. The results showed that nanofluid use as the operating fluid improves the radiative and thermophysical properties, which increases the collector efficiency. In another study, they investigated the effect of discharge on direct absorption solar collectors' efficiency using Al2O3-H2O nanofluids. the collector efficiency for flow rate 1.5 lpm and 2 lpm has increased by 4.2% and 8.1% [12].

Karami et al. [13] investigated the performance of direct absorption solar collectors for residential applications by designing and constructing a device according to EN 2-12975 [14] and built a prototype of this type of collector for domestic water heater use. Experiments were performed with different discharges in the two inner states of the absorber and reflector collectors. The collector efficiency with the adsorbent's internal surface was about 4.11% higher than the reflector's internal surface at 90 l/h flow. To evaluate the collector's performance using metal oxide nanoparticles in the working fluid, they prepared copper oxide nanofluid. They observed that by increasing the nanofluid volume fraction and its discharge, the collector efficiency improves by about 9-17% compared to the base fluid [13]. In the research of *Delfani et al.* [15], it was found that the efficiency of direct adsorption collector using carbon nanotube nanofluid is about 10-29% higher than its efficiency with base fluid. *Vakili et al.* [16] investigated volumetric solar collectors' performance in domestic hot water systems using graphene nanofluid nanofluids. The results showed that the collector efficiency increases

with increasing mass fraction. The best collector efficiency is achieved at a flow rate of 0.015 kg / s for nanofluids and base fluids based on the results. The percentage of efficiency improvement in the mass fraction of 0.005 and the flow rate of 0.015 kg/s compared to the base fluid is 23.2%. Table 1 summarizes the studies performed on solar collectors by direct low-temperature adsorption with nanofluid operating fluid.

Considering the research process on direct solar absorption collectors, it can be concluded that this issue has become one of the topics of interest for various researchers in recent years. On the other hand, following research on nanofluids, researchers have recently begun to use hybrid nanofluids by mixing dissimilar nanoparticles in a base fluid. The idea of using hybrid nanofluids is to further improve the properties of hybrid nanofluids such as heat transfer and pressure drop by considering the advantages and disadvantages of each nanofluid separately [17]. Considering the literature in this field, there is a gap in the comparative studies of different nanoparticles, which can help industry members to select the most suitable nanoparticle in the solar collectors. Another gap is that entropy generation and exergy analysis in nanoparticle systems are very rare and less attractive. This study tries to fill those mentioned gaps and investigates the differences between using different nanofluids and their performance in simulating a solar water heater system with flat plate collectors. For this purpose, copper, copper oxide, and aluminum oxide nanofluid particles have been selected based on water. These nanoparticles are being studied using exergy and energy analysis, and their performance in the solar collector system is compared.

EXPERIMENTAL SECTION

Problem formulation

Fig. 1 shows the geometry of the problem. The two cylinders have constant Temperature boundary conditions, and the Temperature of the inner cylinder is higher than the outer cylinder. Both the inner and outer cylinders rotate at a constant angular velocity in a clockwise and counterclockwise direction [18, 19]. And we consider the clockwise rotation to be negative, and the problem is solved in steady and calm conditions, the nanoparticles with base fluid are in thermal equilibrium conditions, and the relative velocity between them is zero [20].

The thermophysical properties of a fixed fluid are considered, except for the density, calculated using the Bozinsky approximation. Due to the low velocity in the heat transfer phenomenon, the composite displacement term of the viscosity loss in the energy equation has been omitted. The properties of water and nanoparticles can be seen in Table 1. According to this table, it is clear that nanoparticles' thermo-physical properties with a base fluid such as water are very different. The problem is investigated in two-dimensional mode, and the cylindrical coordinate system r is used. The radial coordinates φ start from the upper part of the circular space's vertical axis i n a counterclockwise direction. Dimensional parameters are defined as Eqs (1) and (2) [21, 22].

$$L = r_o - r_i \qquad R = \frac{r}{L} \qquad U_R = \frac{u_r L}{v} \tag{1}$$

$$U_\phi = \frac{u_\phi L}{v} \qquad P = \frac{pL^2}{\rho v^2} \qquad \theta = \frac{T - T_c}{T_h - T_c}$$

$$Gr = \frac{g\beta(T_h - T_c)L^3}{v^2} \qquad Pr = \frac{v}{\alpha} \tag{2}$$

It should be noted that kinematic viscosity is used for dimensionless velocity. Using this method, the velocity is converted to a Reynolds number, which can better interpret the results. The equations of continuity, mass, momentum, and energy are dimensionless as follows [23, 24].

$$\frac{1}{R}\frac{\partial(RU_R)}{\partial R} + \frac{1}{R}\frac{\partial(U_\phi)}{\partial \phi} = 0 \tag{3}$$

$$\frac{1}{R}\frac{\partial(RU_R U_\phi)}{\partial R} + \frac{1}{R}\frac{\partial(RU_\phi U_R)}{\partial \phi} - \frac{U_\phi^2}{R} = \tag{4}$$
$$-\frac{\partial P}{\partial R} + \frac{1}{R}\frac{\partial}{\partial R}\left(R\frac{\partial U_R}{\partial R}\right) + \frac{1}{R^2}\frac{\partial}{\partial \phi}(U_R) - \frac{U_R}{R^2} -$$
$$\frac{2}{R^2}\frac{\partial U_\phi}{\partial \phi} Gr\theta \sin(\phi)$$

$$\frac{1}{R}\frac{\partial(RU_R U_\phi)}{\partial R} + \frac{1}{R}\frac{\partial(U_\phi^2)}{\partial \phi} - \frac{U_R U_\phi}{R} - \tag{5}$$
$$\frac{1}{R}\frac{\partial P}{\partial \phi} + \frac{1}{R}\frac{\partial}{\partial R}\left(R\frac{\partial U_\phi}{\partial R}\right) + \frac{1}{R^2}\frac{\partial^2}{\partial \phi^2}(U_\phi) -$$
$$\frac{U_\phi}{R^2} - \frac{2}{R^2}\frac{\partial U_R}{\partial \phi} = 0$$

$$-\frac{1}{R}\frac{\partial P}{\partial \phi} + \frac{1}{R}\frac{\partial}{\partial R}\left(R\frac{\partial U_\phi}{\partial R}\right) + \frac{1}{R^2}\frac{\partial^2}{\partial \phi^2}(U_\phi) - \tag{6}$$
$$\frac{U_\phi}{R^2} - \frac{2}{R^2}\frac{\partial U_R}{\partial \phi} + Gr\theta\cos(\phi) = 0$$

Border conditions are mentioned as follows [25]:

Table 1: Thermo-physical properties [22].

Parameter	Al_2O_3	Cu	CuO
Density, $kg.m^{-3}$	3890	8978	6000
Heat Constant, $kJ.^oK^{-1}$	880	381	551
Conductivity, mS/cm	35	3876	33

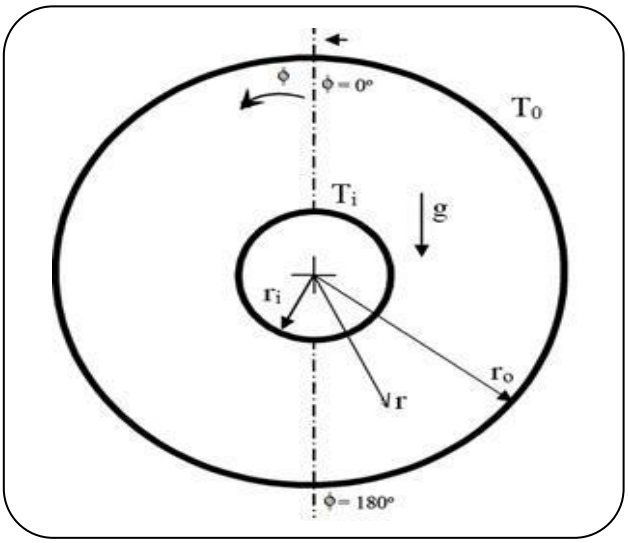

Fig. 1: Problem geometry with various parameters.

$$\begin{cases} R = R_i, & \theta = 1 \\ R = R_o, & \theta = 0 \end{cases} \quad (7)$$

Nanofluid viscosity can be estimated using the basic fluid viscosity based on Equation (8). This equation is proposed for low-concentration suspensions and spherical solid particles by reference [26].

$$\mu_{nf} = \frac{\mu_f}{(1-\varphi)^{2.5}} \quad (8)$$

The density and thermal capacity of nanofluids are calculated using Equations (9) and (10).

$$\rho_{nf} = (1-\varphi)\rho_f + \varphi\rho_s \quad (9)$$

$$(\rho C_p)_{nf} = (1-\varphi)(\rho C_p)_f + \varphi(\rho C_p)_s \quad (10)$$

The thermal conductivity of nanofluids can be estimated using Equation (11); in this relation, n represents the shape coefficient of nanoparticles, and for spherical nanoparticles, its value is equal to 3. The Ref. [27] has proposed this Equation (11).

$$\frac{K_{nf}}{K_f} = \frac{K_S + (n-1)K_f - (n-1)K_f - (n-1)(K_f - K_s)\varphi}{K_s + (n-1)K_f + (K_f - K_s)\varphi} \quad (11)$$

Due to the different epochs of the outer and inner cylinders, the speed limit conditions on these two cylinders are different. According to Equations (12) and (13), the local Nusselt number on two cylinders is defined as dividing the Nusselt number's real in pure conduction mode[28].

$$Nu_i = \frac{-R\frac{\partial\theta}{\partial R}}{Nu_{cond}}, \qquad R = R_i \quad (12)$$

$$Nu_O = \frac{-R\frac{\partial\theta}{\partial R}}{Nu_{cond}}, \qquad R = R_O \quad (13)$$

Nu_{cond} represents the Nusselt number under net conduction heat transfer conditions in the above equations and is defined as Equation (14).

$$Nu_{cond} = \frac{1}{\ln(\frac{r_o}{r_i})} \quad (14)$$

The mean Nusselt number is obtained by integrating the local Nusselt number around the cylinders as Equations (15) and (16) [29].

$$\overline{Nu_i} = \frac{1}{2\pi}\int_0^{2\pi} Nu_i(\phi)d\phi \quad (15)$$

$$\overline{Nu_o} = \frac{1}{2\pi}\int_0^{2\pi} Nu_o(\phi)d\phi \quad (16)$$

Also, the algorithm of the numerical simulation of the system is shown in Fig. 2.

Geometry and numerical method

Fig. 3 shows the networked geometry of the problem. The governing equations are solved using the finite volume method based on the simple algorithm [30-33]. The pressure equation's discretization is done using the standard method, and the momentum energy equations are done using the first-order upstream method. Is. The following discount coefficients for pressure, density, buoyancy force, momentum, and energy are about 0.2 to 1. The number of iterations to converge under different conditions is about 2000 iterations, and the residuals for the equations of continuity, momentum, and energy are equal to 10^{-9}, 10^{-11}, and 10^{-15}, respectively.

In this study, the upper part of the collector is continuously absorbing solar energy while the collector's sides' vertical plates are insulated, and the lower plate

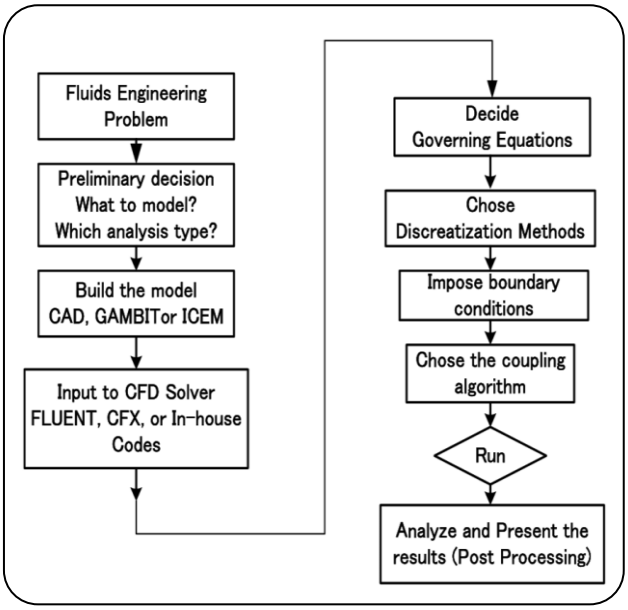

Fig. 2: Typical algorithm of computational fluid dynamics solutions.

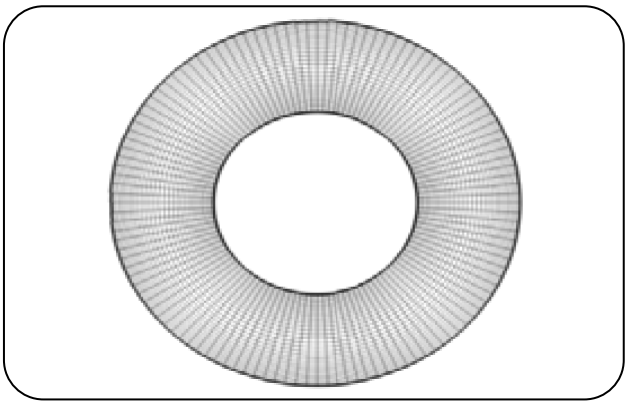

Fig. 3: Example of a computational network.

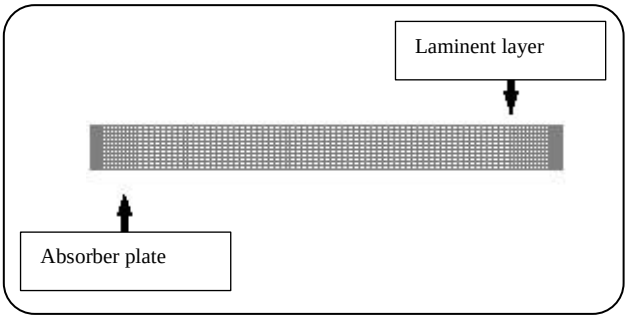

Fig. 4: shows a mesh in the two-dimensional channel of the desired results and a discussion of the geometry of the problem.

of the collector is kept constant at T_c Temperature. High-level concentrations are also considered higher than low-level is assumed($C_c < C_h$). The nanoparticles are assumed to be spheres with a diameter of 5 nm and the amplitude of the wave A_m=0.04 m, and the value of the wavelength $\lambda = 3.5$ for the absorber plate (Fig. 4) [34-36].

The two-dimensional steady-state channel is designed with insulation walls on either side. Solar energy radiation is absorbed by its top cover and directed to the absorber plate. It is located inside the nanofluid system, and its particles move due to heat transfer. To check the mesh's quality, the element's quality is a function of the scales being measured and is very suitable for estimating the mesh conditions created [37-43].

Independence from the network and validation of the numerical solution

To ensure that the results are not dependent on the grid size, the value of the local Nusselt number on the inner cylinder for conditions Pr = 0.7 using three grids of 15×60, 30×120, and 240×60 for normal displacement under the conditions specified in Fig. 5. Extracted and compared. Table 2 shows the mean Nusselt number values in the conditions of Fig. 5. According to the table, it is clear that the mean Nusselt number values in different networks are less than four percent different. The set of solutions performed in this study was performed using the mentioned network[44-49].

System modeling

Solar Collectors consist of a control system, a flat panel solar collector, an energy storage tank, a pump, a flow separator, and a flow integrator. The absorber plate is the main component of the solar collector through which the action of absorbing solar radiation and transferring heat to the operating fluid is done. The absorber plate should have high thermal conductivity, high radiation absorption coefficient, low emission coefficient, and resistance to internal and external corrosion. The tank's energy dissipation coefficient is very important because it determines how fast the obtained energy is lost. The lower the value, the better the tank performance. When there is no current, some of the energy obtained is lost due to heat transfer from the walls to the outside and energy loss. Some of the heat generated is not solar and is provided by an auxiliary heat exchanger built into the energy storage tank. The number of auxiliary heat exchangers can also be determined. When a lot of energy is needed, only a heat exchanger is turned on, and this design is disabled

Table 2: Network size and average Nusselt number.

Network size(r×ϕ), mm^2	Mean Nusselt
15×60	1.1801
30×120	1.1791
60×240	1.1071

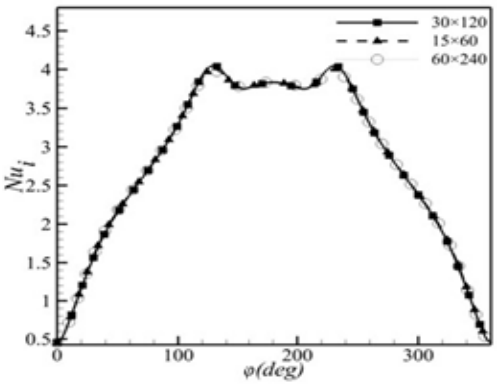

Fig. 5: Mesh dependency analysis.

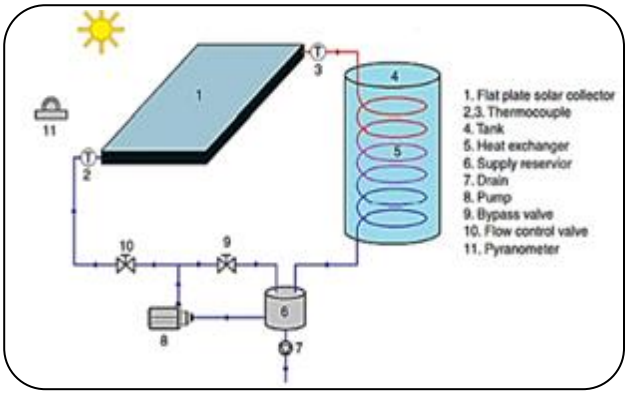

Fig. 6: Schematics of a solar water heater .

in the water storage tanks of water heaters. The heat transfer fluid must have a high specific heat capacity, low heat dissipation coefficient, high heat transfer, low viscosity, and no corrosion. The price of the fluid is very important, which should ultimately be affordable. Different nanofluids' behavior and efficiency have been investigated according to Temperature, velocity distribution, radiant heat transfer, and convection (Fig. 6) [50-53].

In simulating the system with TRNSYS software, the weather information of the area or city understudy is needed. Therefore, two cities of Bandar Abbas and Tabriz have been selected from the eight cities whose information was available. Thus, each nanofluid's performance and comparison with other nanofluids is also examined in different climatic conditions. Introducing long times with short time intervals will lead to crowded charts, so the middle day is considered the year's hottest month (Table 2).

Energy and Exergy Analysis

Investigating the energy of a solar water heater system The amount of useful energy collected is obtained through Equations (17) and (18).

$$Q_{useful} = Q_{recv} - Q_{loss} = AI(\lambda k) - hA(T_{col} - T_{amb}) \quad (17)$$

$$Q_{useful} = mc_p(T_{out} - T_{in}) \quad (18)$$

Where λ = surface displacement rate, k = adsorption rate by adsorbent, T_{out} = collector output Temperature, T_{in} = collector inlet Temperature, T_{col} = collector Temperature, and T_{amb} = ambient Temperature. F_R is a coefficient used to express the collector's efficiency and the ratio of actual useful energy to useful heat when the Temperature is the average Temperature of the fluid inside the collector.

$$F_R = \frac{mC_p(T_{out} - T_{in})}{AI(\lambda k) - hA(T_{col} - T_{amb})} \quad (19)$$

The flat panel solar collector's efficiency, which is the ratio of useful energy to solar energy, is calculated.

$$\eta = \frac{mc_p(T_{out} - T_{in})}{AI} \quad (20)$$

$$\eta = \frac{\left(F_R AI(\lambda k) - F_R hA(T_m - T_{amb})\right)}{AI} = F_R(\lambda k) - F_R h\left(\frac{T_m - T_{amb}}{I}\right) \quad (21)$$

With the help of Navier Stokes equations for energy and concentration, a solar collector can be modeled. The state equations with the corresponding boundary conditions are transformed into a dimensionless form and are solved numerically by the finite difference method.

Also, Exergy equations are used in the system to obtain exergy values. This Equation (22) is generally defined for solar flat panel collectors [38]:

$$Ex_{in} + Ex_s + Ex_{out} + Ex_d = 0 \quad (22)$$

The input exergy rate consists of two parts: the input exergy rate based on fluid flow and the input exergy rate based on the radiative exergy rate. The input exergy rate based on fluid flow is defined as Equation (23) [6]:

Table 3: Specifications of the energy storage tank.

	Parameter	assumption
storage tank	Volume	0.3 m^3
	Heat loss coefficient	2.5 $kJ.hm^{-2o}K^{-1}$
separator	Inlet mass flow	100kg/h
	Reservoir Temperature	55 C
	Control Temperature	45C

$$Ex_{in} = mc_p\left(T_{in} - T_a - T_a Ln\left(\frac{T_{in}}{T_a}\right)\right) \quad (23)$$

The exergy rate of absorbed radiation, which is part of the input exergy, is defined as Equation (24) [6]:

$$Ex_s = \eta_o G_t A_p\left[1 - \left(\frac{T_a}{T_s}\right)\right] \quad (24)$$

Ts is the sun's temperature, G_t is glass transparency and A_p is the area of the collector. The sun's surface Temperature is equal to 5700 ^oK. The system is considered a bulk body in the above relation. The exergy rate of outlet fluid is described as follows:

$$Ex_{out} = mc_p\left[T_{out} - T_a - T_a Ln\left(\frac{T_{out}}{T_a}\right)\right] \quad (25)$$

Degraded exergy rate The collector itself consists of three degraded exergy rates according to Equation (27) [39]:

$$Ex_d = Ex_{d,T_s} + Ex_{d,P} + Ex_{d,T_f} \quad (26)$$

As the degraded exergy due to the Temperature difference between the collector surface and the sun surface is equal to:

$$Ex_{d,T_s} = -\eta_o G_t A_p T_a\left(\frac{1}{T_p} - \frac{1}{T_s}\right) \quad (27)$$

The adsorbent surface of the collector is introduced to the surrounding environment, the rate of exergy wasted due to heat loss with the environment, which is introduced by the following Equation (28) [6]:

$$Ex_{d,T_f} = -U_L A_p T_a\left(T_p - T_a\right)\left(1 - \frac{T_a}{T_p}\right) \quad (28)$$

Finally, the degraded exergy due to pressure drop in the collector is equal to [6]:

$$Ex_{d,p} = -\frac{m\Delta P}{\rho} \quad (29)$$

In the above relations, c_p is the heat capacity of the fluid used in the collector, which in the case of using nanofluid, the heat capacity of the nanofluid is obtained from equation (30) [40]:

$$C_{p,nf} = \frac{\phi\left(\rho_{np}C_{pnp}\right) + (1-\phi)\left(\rho_{bf}C_{pbf}\right)}{\phi\rho_{np} + (1-\phi)\rho_{bf}} \quad (30)$$

In this regard, the mass fraction of nanofluid and C_{pbf}, ρ_{bf} And the heat capacity and density of the base fluid and C_{pnp} and ρ_{np} are the heat capacity and density of the nanoparticles, respectively. The solar flat plate collector's exergy efficiency is defined as the difference between the inlet and outlet exergy of the operating fluid flow on the radiative exergy by the radiation source [17].

$$\eta_{ex} = \frac{c_p\left[T_{out} - T_a - T_a Ln\left(\frac{T_{out}}{T_a}\right)\right]}{G_t A_p\left[1 - \frac{T_a}{T_s}\right]} \quad (31)$$

To evaluate the exergy efficiency, one must first examine the different exergy rates in the solar flat plate collector.

RESULTS AND DISCUSSION

Collector simulation results

In this study, the problem was calculated using a pressure-based solver, independent of time. The PISO procedure was used despite the higher computational cost due to the higher accuracy of the calculations. The system will be solved in the state of natural displacement. Depending on the flow rate, the solution will be turbulent or laminar. In this modeling, due to the natural displacement, the flow will be laminar. Finally, the continuity equations, velocity equations in two directions, energy equations, and radiation equations were studied and converged. The estimations' accuracy is 10^{-6} for the energy and radiation equations and 10^{-3} for the software's velocity and continuity equations. The results of the simulation are shown in Figs. 7-10.

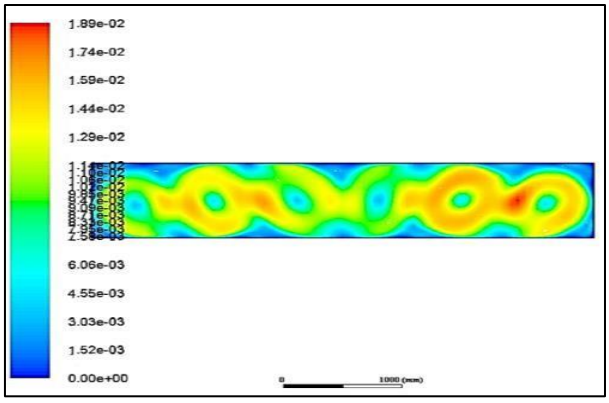

Fig. 7: Velocity of natural circulation using water.

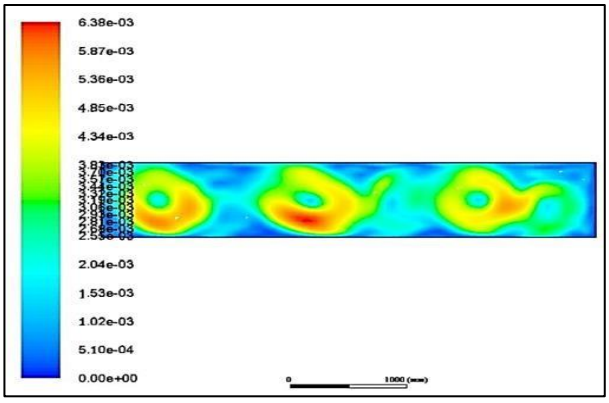

Fig. 9: Velocity f natural circulation using copper oxide nanofluid.

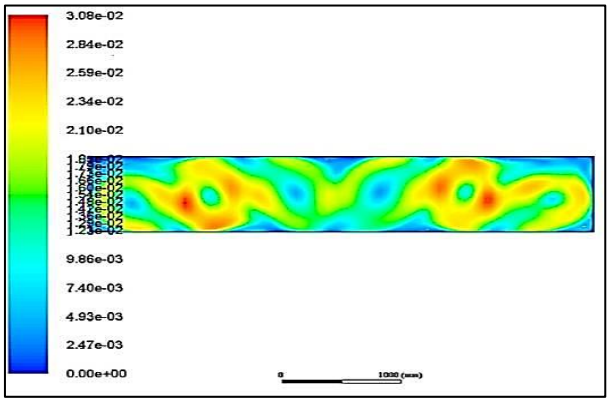

Fig. 8: Natural circulation velocity using aluminum oxide.

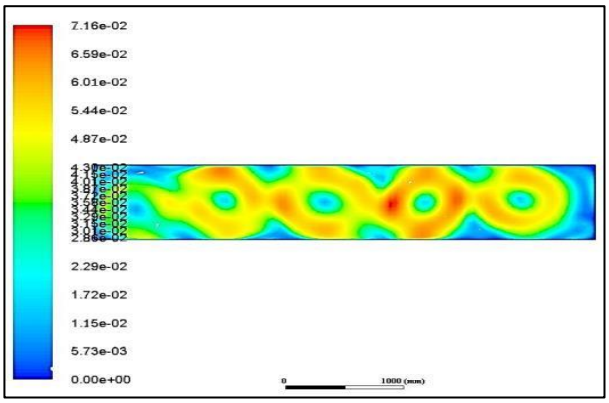

Fig. 10: The velocity of natural circulation using copper nanofluid.

By creating heat transfer and increasing sunlight absorption, the circular motion inside the diffuser has increased the heat transfer to the absorber plate; by changing the fluid to alumina nanofluid, the nanofluid's velocity inside the diffuser increases. The relative symmetry remains, and the system seeks to increase the heat transfer from the cover plate to the absorber plate by increasing the rotational period created. The conversion of the nanofluid used by aluminum oxide to copper oxide has caused a more circulating current inside the diffuser and increased nanofluid movement speed. The highest velocity is shown in the center of the rotation towards the absorber plate. Due to its high heat transfer coefficient, copper nanofluid has increased the adsorbent's Temperature by absorbing more heat transfer than copper oxide, aluminum oxide, and water-based nanofluids.

The authors have calculated the free convective heat transfer coefficient of nanofluids in theoretical and experimental results were compared and also evaluate the effect of particle concentration and operating Temperature on the forced convective heat transfer coefficient of nanofluids. The comparison of theoretical and simulated results is shown in Figs. 11 and 12.

Collector system performance

The results are analyzed by comparing the diagrams of different nanofluids in the two cities' climatic conditions (Figs. 13 and 14). Nanofluids containing copper oxide and aluminum oxide particles reach lower Temperatures, and as the flow is faster, the higher the Temperature, the faster the nano-particles with copper particles reach the desired maximum Temperature of 100 ° C.

The amount of sunlight on the collector surface is constant in a weather condition. In Tabriz's city, the water's Temperature leaving the collector is much higher than the water Temperature, leaving the collector in Bandar Abbas's city (Figs. 15 and 16).

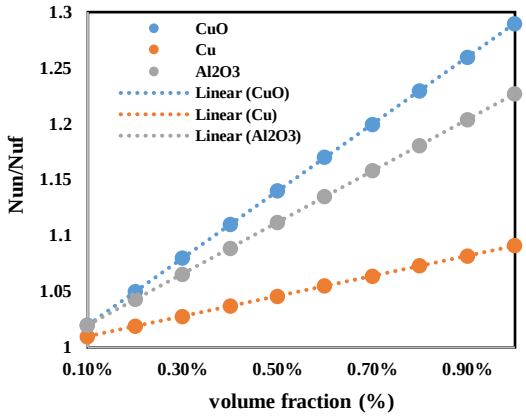

Fig. 11: The new Nusselt number of fluid mixed with CuO, Cu, and Al_2O_3 nanofluids compared to the former fluid without mixing particles in plate collector.

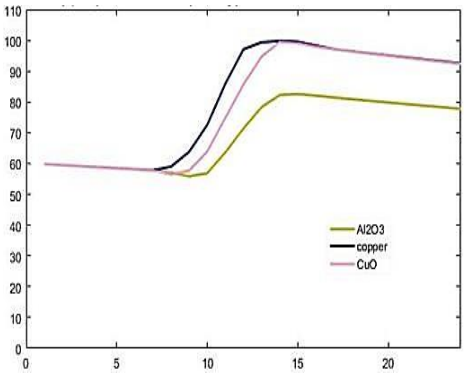

Fig. 13: Diagram of the final Temperature of the outlet water for three nanofluids in Bandar Abbas.

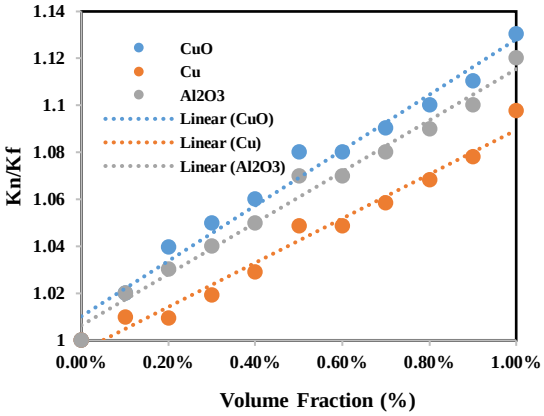

Fig. 12: The new linear thermal conductivity of fluid mixed with CuO, Cu, and Al_2O_3 nanofluids compared to the former fluid without mixing particles in plate collector.

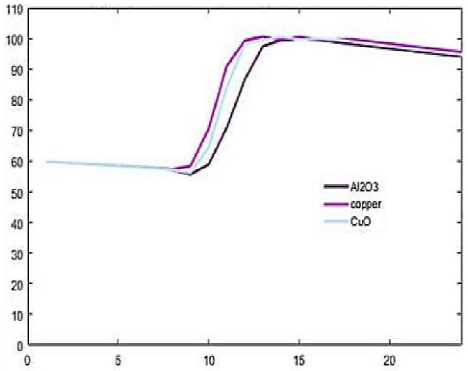

Fig. 14: Diagram of the final outlet water Temperature for three nanofluids in the city of Tabriz.

The outlet water Temperature is the maximum Temperature at which the collector can heat water utilizing solar and nanofluid energy. The Temperature is regulated by a controller connected to the collector and reaches the consumer up to a maximum of 100 ° C. Nanofluid with copper particles has the highest output Temperature. In other words, a solar collector with copper nanofluid can increase the water Temperature further, and finally, the output water from it has a higher Temperature than other nanofluids. It is noteworthy that the solar collector using nanofluid in Tabriz can increase the Temperature more than Bandar Abbas. The ambient Temperature diagrams of each city are shown in Fig. 17, and it is clear that the city of Bandar Abbas has a higher ambient Temperature than the city of Tabriz. Tabriz's city has a higher altitude, less air concentration, and more sunlight on the collector surface.

Because the maximum output Temperature is 100 ° C, this system can be used for nanofluids with copper particles in both cities. As shown in the diagrams, if nanofluids with aluminum oxide particles are used in Bandar Abbas, Because the maximum water outlet Temperature is 83 ° C, a heat exchanger must be used to achieve the desired Temperature is 100 ° C. It should be noted that there are different types of auxiliary heaters and the heater used here with Depending on the amount of energy, when the Temperature reaches 55 ° C, it turns on. It heats the water to 60 ° C. Water at a Temperature below 100 ° C leaves the collector and enters the energy storage tank heated by a heat exchanger and delivered

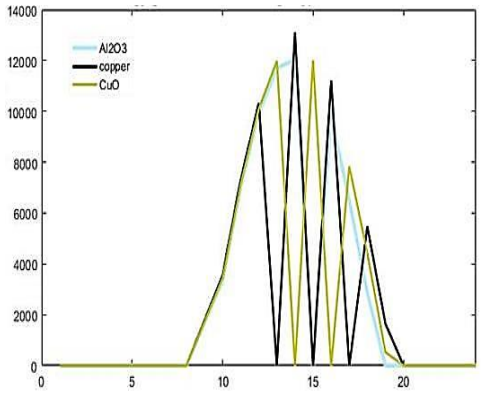

Fig. 15: Chart of useful collector energy for three nanofluids in the city of Tabriz.

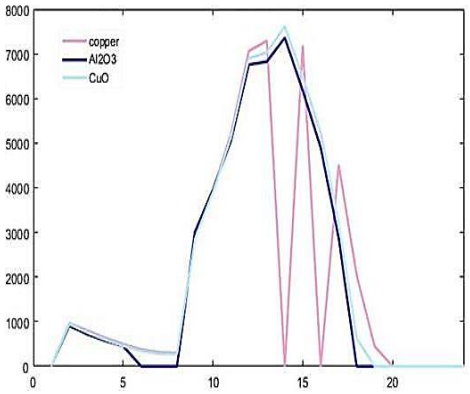

Fig. 16: Chart of useful collector energy for three nanofluids in Bandar Abbas.

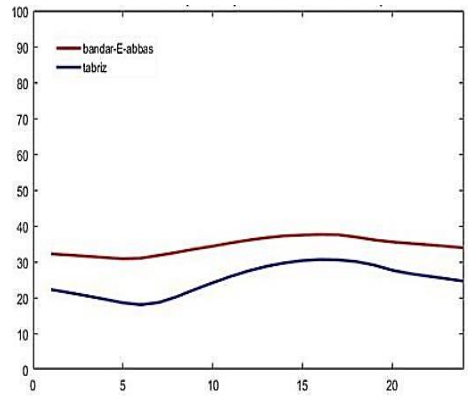

Fig. 17: Diagram of ambient Temperature in Bandar Abbas and Tabriz.

Table 4: Value of input to the system in the simulation.

Schedule	Mass flow, $kg.h^{-1}$
7-9 am	0.1
9 am-3 pm	0.2
3 pm-6pm	0.1

Table 5: The amount of flow applied to the system in the simulation.

Schedule	Mass flow of stream 4, $kg.h^{-1}$	Mass flow of stream 5, $kg.h^{-1}$
7 - 9 am	1	1
9 am - 3 pm	2	4
3 pm-6 pm	1	2

to the consumer. For aluminum oxide nanofluids with the mentioned water Temperature, after leaving the collector, the Temperature does not drop to 55 ° C, which forces the system to turn on the heat exchanger. But it is normal for a slight drop to leave the energy storage tank and reach the consumer. Part of the decline is also due to the storage tank dissipation coefficient discussed earlier. Finally, the consumer Temperature using aluminum oxide nanofluid in Bandar Abbas will be 80 ° C. The input \and applied flow values are presented in Tables 4 and 5.

Water flow discharge: After applying the new inlet water flow, due to the increase in the inlet water's mass flow, the system needs auxiliary energy to heat all the incoming water and use only solar energy nanofluid used in it will not respond to increasing water Temperature (see Figs. (18 and 19)).

The collector outlet Temperature decreased with increasing inlet water flow. The sun's energy and the fluid used in the system are the same, and when more water enters the system, the said energy will heat a smaller volume of water to the desired Temperature or increase the total incoming water at a lower Temperature. When the flow rate increases by 20, the result is an increase in auxiliary heat energy. After the heat exchanger raises the water temperature to an acceptable level, it shuts down, and the solar energy system continues to increase the Temperature until it reaches the maximum Temperature. According to the diagram, the Temperature of different points of the energy storage tank also fluctuates. It can be concluded that if the heat exchanger and solar collector power and the amount of solar,

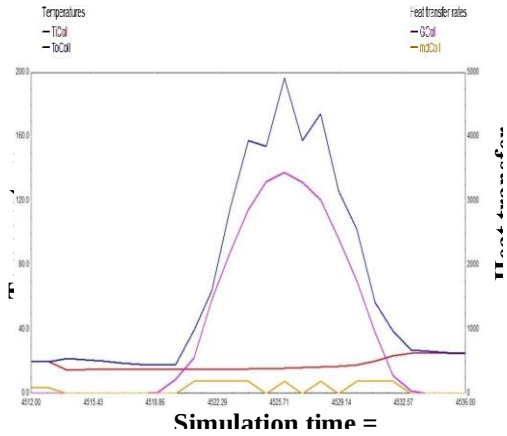

Fig. 18: Diagram of water Temperature coming out of the collector in the applied flow No. 4.

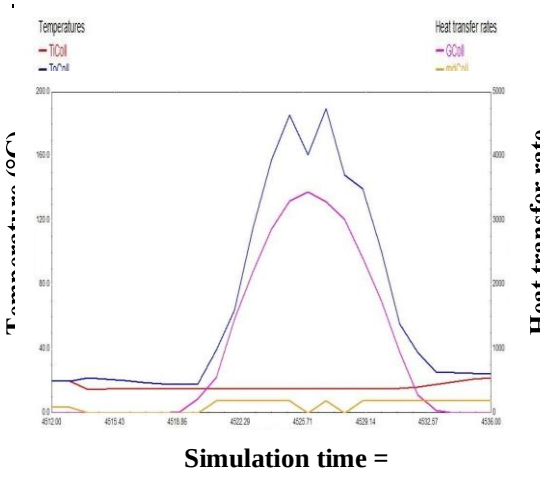

Fig. 19: Graph of outlet water Temperature from the collector in the applied flow No. 5.

radiation remain constant with increasing the mass flow rate of the incoming water, the system Temperature fluctuation increases, The heat exchanger is switched on. Its energy will increase in proportion to the amount of inlet flow, and the final Temperature will be slightly lower than the maximum Temperature. If the heat exchanger power is increased, the maximum Temperature can be reached. The area applied to the collector surface in the simulation is presented in Table 6. The level intended for the collector in the simulation is 2 (A_c =5m). The outlet water Temperature diagrams are presented in Figs. 20 and 21.

The higher the collector level, the sooner the desired Temperature will be reached. Increasing the level of collectors has a positive effect on the system, and of course, this change requires an optimal economic impact. Since the three nanofluids studied in previous studies have not been analyzed together, the study of Nusselt number changes can be good evidence of how they work compared to each other. Nusselt number changes are observed based on the amount of heat transfer, which is greater when using copper nanofluids. Heat transfer within the diffuser is free-moving, and improved Nusselt number changes along the diffuser result in better and more orderly velocity profiles(see Figs. 22).

Nanofluids are a mixture of metal nanoparticles or metal and carbon oxides that have been mixed to improve the thermal and physical properties of the base fluid. Many fluids are used in industry, and the range of these fluids range is limited due to physical and safety limitations in some cases. Therefore, the relevant fluid can not completely meet the existing needs. A good example of this is low-Temperature thermal cycles or organic Rankine cycles that work with organic fluids or solar thermal systems suitable for this type of cycle. These fluids are very suitable for these cycles due to the low boiling point, but they have low thermal efficiencies due to their low thermal conductivity. Therefore, if this defect can be solved by adding nanoparticles with high thermal conductivity, higher powers can be achieved in these cycles, and more energy can be transferred through this. This project investigates the effect of using nanofluids on improving the performance and thermal efficiency of the organic cycle. To be able to determine how much heat transfer and production work can be improved if nanofluid is used instead of the primary fluid in this cycle, and in a broader sense, by examining the exergy efficiency, the effect of this effect on converting available work into useful work can be investigated.

Fig. 23 shows the variations of different exergy rates for different nanofluids with a mass percentage of 3.0% at a flow rate of 2 liters per minute. As shown in Fig. 23, as the amount of radiation on the collector surface increases, increasing the collector surface Temperature and the operating fluid Temperature, the exergy rates' values all increase. For the two exergy curves of absorbed radiation and degraded exergy due to the difference between the collector surface Temperature and the surface Temperature of the sun, the values of these two exergy rates are higher than the other values of the exergy rates and with increasing radiation, these two exergy rates increase significantly. The exergy rates of degraded and

Table: 6 Area applied to the collector level in the simulation.

Area	Optimum value
Area 1	10 m^2
Area 2	7.5 m^2
Area 3	2.5 m^2

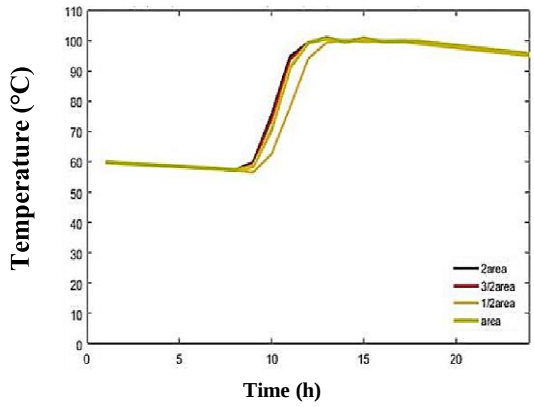

Fig. 20: Graph of the final Temperature of the water leaving the system for the consumer in different areas of the collector.

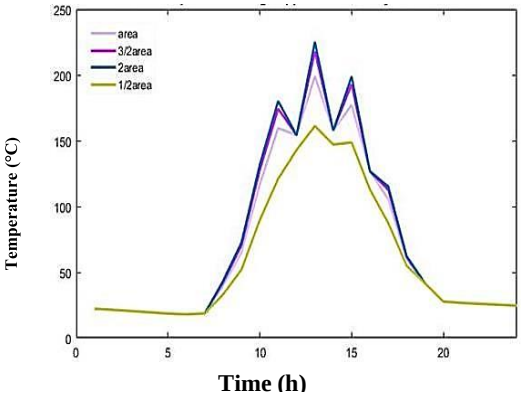

Fig. 21: Graph of the outlet water Temperature in the collector in different areas of the solar collector.

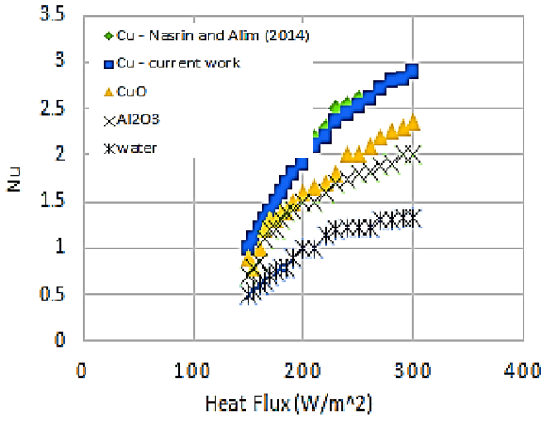

Fig. 22. Graph of Nusselt number changes per unit length of diffuser in terms of the heat transfer value.

leaked and the difference in the inlet and outlet of the collector operating fluid are relatively smaller. The exergy rate of inlet and outlet increases with increasing radiation due to the difference between the inlet and outlet Temperatures of the collector's fluid. In this diagram, due to the slight pressure drop of the collector's fluid, the amount of degraded exergy rate due to the pressure drop due to its very small amount (less than one watt) is indicated at the bottom of the diagram.

According to the exergy efficiency relations, the amount of efficiency in the days and different hours of the simulation in 30-minute intervals for the discharges and the percentage of different nanofluid masses has been calculated. In Fig. 24, the amount of exergy efficiency at different times of the day is shown according to radiation and ambient Temperature. From Fig. 24, it is shown that with increasing the amount of radiation and as a result of the average collector surface Temperature, the amount of collector exergy efficiency increases. Also, by adding different nanoparticles to the base fluid (water), the exergy efficiency significantly increased. Also, in Fig. 25, the solar collector's efficiency is simulated for nanofluids' different volume fractions.

Although many experimental and theoretical studies have been performed on nanofluids' thermal properties, very few of these studies have examined nanofluids based on the fluids used in collectors, and this number is much lower in experimental studies. *Wang et al.* [13], in an experiment, investigated the production methods of nanofluid-containing gold particles in therminol VP1 and this nanofluid's thermal properties. For mass concentrations of 0.005%, 0.01%, and 0.05% in this study, the increase in thermal conductivity was equal to 4.8% and 6.5%, respectively. Using the relationships presented for thermal conductivity used in this modeling, the percentage increase of nanofluid thermal conductivity at 30 °C, 3.6, 3.1, and 7.38, respectively, is obtained for these mass concentrations. In Fig. 26, the experimental values are obtained. And the theory for different nanofluids studied in this research can be compared [13-16].

CONCLUSIONS

In the present paper, solar thermal system are simulated and their exergy and economic analysis is performed. The working fluid of the solar thermal system is Al2O3/water nanofluid flowing in a specific arrangement of copper tubes.

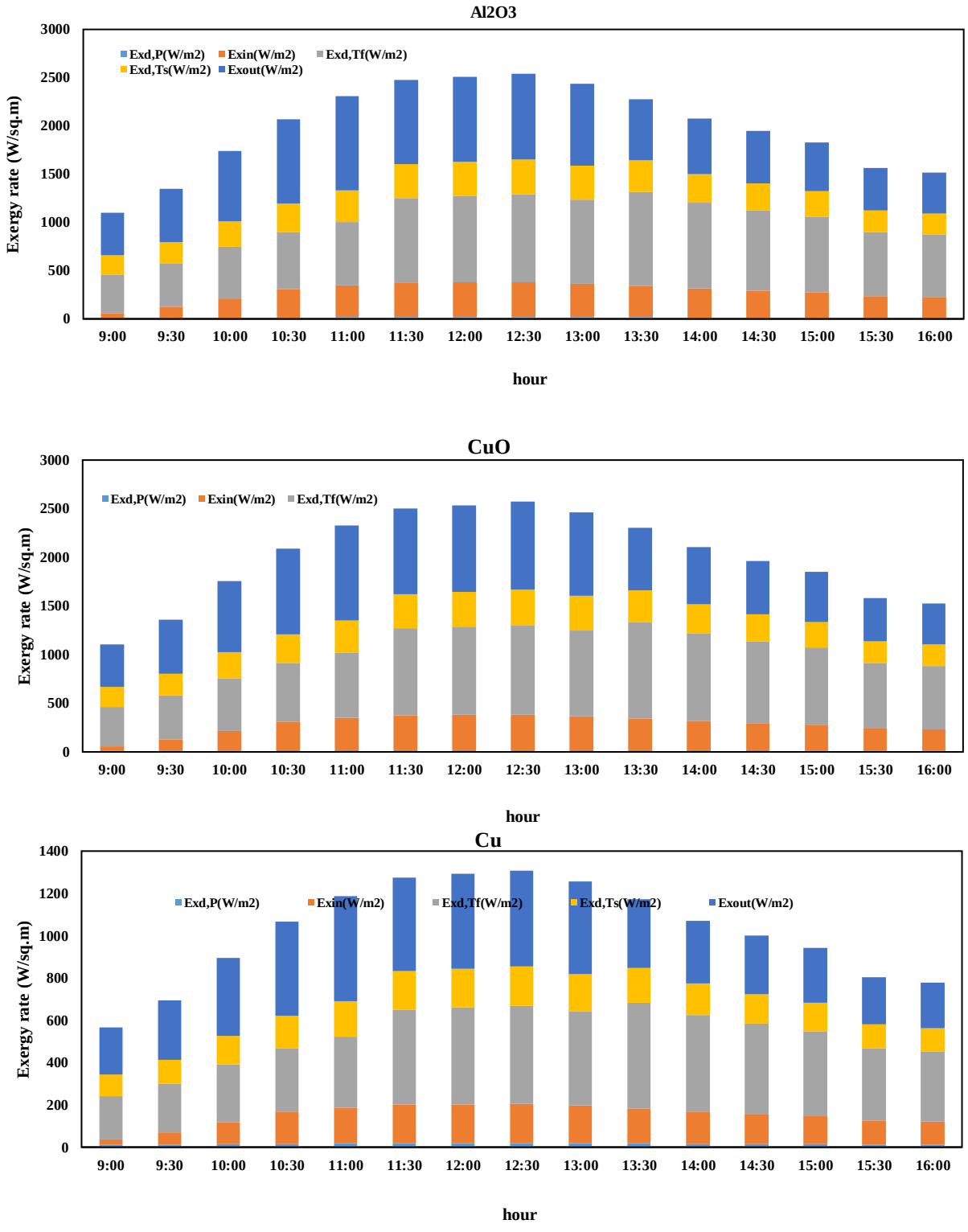

Fig. 23: Changes in the exergy rates of absorbed radiation and degraded exergy due to the difference between the Temperature of the sun and the collector surface, the leaked exergy, the exergy due to the fluid flow, and the difference between the collector surface Temperature and the fluid Temperature, and the difference between the exit and inlet exergy rates in (a) Al_2O_3 (b) CuO (c) Cu nanoparticles.

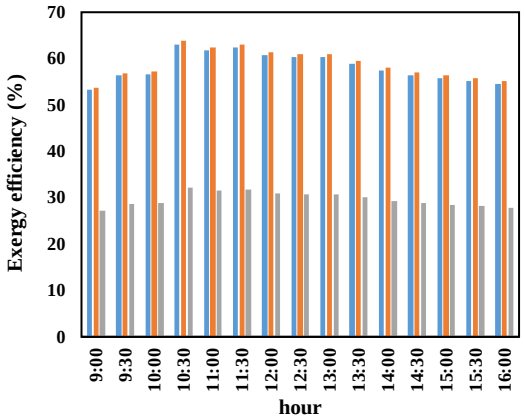

Fig. 24: Exergy efficiency variances according to irradiance duration and ambient Temperature in different day hours at the base fluid mode with a volumetric flow rate of 1.5 liters/minute.

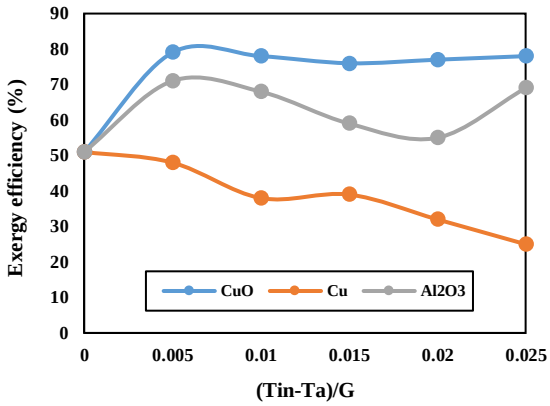

Fig. 25: The efficiency of the Flat plate collector system of CuO, Cu, and Al2O3 Nano Fluids.

By changing the Q and φ, the amount of exergy output, exergy efficiency, and investment recovery time are analyzed and the following results are obtained. An increment in the working flow rate in the heat exchanger system in solar thermal, cools more the panel. Enhancing the fluid flow rate in the heat exchanger system in solar thermal reduces exergy output. Increasing the volume percentage of nanoparticles enhances the exergy output. The maximum exergy output is obtained for 1% nanofluid at a flow rate of 0.5 lit/min. An enhancement in the fluid flow rate of the heat exchanger system in solar thermal reduces the exergy efficiency so that increasing the water flow rate from 0.5 to 4 lit/min reduces the exergy efficiency by 2.03%. The addition of nanoparticles enhances the exergy efficiency so that adding 1% Al_2O_3 to water at a flow rate of 0.5 lit/min enhances the exergy efficiency by 0.45%. Maintenance cost and the initial cost of solar thermal system is more than PV, while investment recovery is 6 years for PV and 4 years for solar thermal. According to the case study, this study can be done for different countries to obtain estimation for the efficiency of solar systems economically. Besides, other cooling systems can be evaluated for the solar panel to investigate its effect on solar thermal exergy output. The comparison of nanofluid mixtures and water used in this study and their changes compared to copper nanofluid in another study shows that nanofluid with copper particles has the best performance and exergy efficiency than other nanofluids. Collectors in cold climates using these nanoparticles have led to attaining more energy from the sunlight. As the inlet water flow rate increases, the collector efficiency increases, and as the solar collector level increases, the amount of radiation absorbed from the sun increases, which will ultimately lead to increased efficiency. Comparing the results obtained for solar collectors, it can be seen that the efficiency of solar water heaters has increased significantly. The changes in velocity obtained in modeling the system using water fluid with the results obtained from previous studies are somewhat acceptable, and there is a slight change due to the lack of the same diffuser length and a difference in the mesh structure of the two studies. Similarly, other changes obtained for nanofluids in modeling can be considered acceptable. The flow exergy for the three nanofluids of copper oxide, aluminum oxide, and copper is calculated to be 67%, 57%, and 53%, respectively. The portion of the nanofluid energy of aluminum oxide that can be converted to work will be greater. According to the studies, it is clear that energy efficiency and exergy in many cases are opposite to each other. In this study, energy efficiency for three nanofluids of copper oxide, aluminum oxide, and copper have been calculated 76%, 67%, and 48%, respectively. Results also show that increasing the inlet water Temperature decreases the collectors' energy efficiency and generally increases the exergy efficiency to its maximum value.

Nomenclature

D	Internal cylinder diameter, m
g	Gravity acceleration
Gr	Graf number
L	Characteristic length, m

Nu	Nusselt number
P	Dimensionless pressure
p	Pressure, kg/m.s^2
Pr	Prandtl number
R	Dimensional radial coordinates
c	Cold
h	Hot
f	Fluid
i	Inlet
o	Outlet
r	Radius, m
Ra	Riley number
Re	Reynolds number
Ri	Richardson's number
T	Temperature, ^{o}K
U	Velocity, m/s
U	Dimensionless velocity
β	Expansion coefficient, ^{o}K^{-1}
Θ	Temperature without dimension
μ	Dynamic viscosity, kg/m.s
υ	Cinematic viscosity, m^2/s
ρ	Density, kg/m^3
ϕ	Tangential coordinates
φ	Volume percentage of nanoparticles

Received : Apr. 7, 2022 ; Accepted : June 13, 2022

REFERENCES

[1] Arai N., Itaya Y., Hasatani M., Development of a "Volume Heat-Trap" Type Solar Collector Using a Fine-Particle Semitransparent Liquid Suspension (FPSS) as a Heat Vehicle and Heat Storage Medium Unsteady, One-Dimensional Heat Transfer in a Horizontal FPSS Layer Heated by Thermal Radiation, *Solar Energy*, **32(1)**: 49-56 (1984).

[2] Taylor R. A., Phelan P. E., Otanicar T. P., Adrian R., Prasher R., Nanofluid Optical Property Characterization: Towards Efficient Direct Absorption Solar Collectors, *Nanoscale Research Letters*, **6(1)**: 1-11 (2011).

[3] Minardi J. E., Chuang H. N., Performance of a "Black" Liquid Flat-Plate Solar Collector, *Solar Energy*, **17(3)**: 179-183 (1975).

[4] Tyagi H., Phelan P., Prasher R., Predicted Efficiency of a Nanofluid-Based Direct Absorption Solar Receiver, *Journal of Solar Energy Engineering*, **131**: 729-736 (2009).

[5] Otanicar T.P., Phelan P.E., Prasher R.S., Rosengarten G., Taylor R.A., Nanofluid-Based Direct Absorption Solar Collector, *Journal of Renewable and Sustainable Energy*, **2(3)**: 033102 (2010).

[6] Otanicar T.P., Golden J.S., Comparative Environmental and Economic Analysis of Conventional and Nanofluid Solar Hot Water Technologies, *Environmental Science & Technology*, **43(15)**: 6082-6087 (2009).

[7] Howe M.L., Paul T.C., Khan J.A., Radiative Properties of Al2O3 Nanoparticles Enhanced Ionic Liquids (NEILs) for Direct Absorption Solar Collectors, *Solar Energy Materials and Solar Cells*, **232**: 111327 (2021).

[8] Bandarra Filho E.P., Mendoza O.S.H., Beicker C.L.L., Menezes A., Wen D., Experimental Investigation of a Silver Nanoparticle-Based Direct Absorption Solar Thermal System, *Energy Conversion and Management*, **84**: 261-267 (2014).

[9] Parvin S., Nasrin R., Alim M.A., Heat Transfer and Entropy Generation through Nanofluid Filled Direct Absorption Solar Collector, *International Journal of Heat and Mass Transfer*, **71**: 386-395 (2014).

[10] Gupta H.K., Agrawal G.D., Mathur J., An Experimental Investigation of a Low Temperature Al2O3-H2O Nanofluid Based Direct Absorption Solar Collector, *Solar Energy*, **118**: 390-396 (2015).

[11] Kim J., Kang Y.T., Choi C.K., Analysis of Convective Instability and Heat Transfer Characteristics of Nanofluids. *Phys. Fluids*, **16(7)**: 2395-2401 (2004).

[12] Izadkhah M., Erfan-Niya H., Moradkhani H., Rheological Behavior of Water-Ethylene Glycol Based Graphene Oxide Nanofluids, *Iranian Journal of Chemistry and Chemical Engineering (IJCCE)*, **37(5)**: 177-187 (2018).

[13] Wang X., Xu X., Choi S.U.S., Thermal Conductivity of Nanoparticle-Fluid Mixture, *J. Thermophys. Heat Transfer*, **13**: 474-480 (1999).

[14] Mokhtari Ardekani A., Kalantar V., Heyhat M.M., Experimental Study on Heat Transfer Enhancement of Nanofluid Flow Through Helical Tubes, *Advanced Powder Technology*, **30(9)**: 1815-1822 (2019).

[15] Radkar R.N., Bhanvase B.A., Barai D.P., Sonawane S.H., Intensified Convective Heat Transfer Using ZnO Nanofluids in Heat Exchanger with Helical Coiled Geometry at Constant Wall Temperature, *Materials Science for Energy Technologies*, **2(2)**: 161-170 (2019).

[16] Jumpholkul, C., Asirvatham, L.G., Dalkılıç, A.S., Mahian, O., Ahn, H.S., Jerng, D.W., Wongwises, S., Experimental Investigation of the Heat Transfer and Pressure Drop Characteristics of SiO_2/Water Nanofluids Flowing Through a Circular Tube Equipped with Free Rotating Swirl Generators, *Heat and Mass Transfer*, 1-19 (2019).

[17] Keblinski P., Phillpot S.R., Choi S.U.S., Eastman J.A., Mechanisms of Heat Flow in Suspensions of Nano-Sized Particles (Nanofluids), *Int. J. Heat Mass Transfer*, **45(4)**: 855-863 (2002).

[18] Pinto R.V., Fiorelli F.A.S., Review of the Mechanisms Responsible for the Heat Transfer Enhancement Using Nanofluids, *Appl. Therm. Eng.*, **108**: 720-739 (2016).

[19] Li C., Peterson G., Mixing Effect on the Enhancement of the Effective Thermal Conductivity of Nanoparticle Suspensions (nanofluids), *Int. J. Heat Mass Transfer*, **50(23)**: 4668-4677, (2007).

[20] Jang S.P., Choi S.U.S., Role of Brownian Motion in the Enhanced Thermal Conductivity of Nanofluids, *Appl. Phys. Lett.*, **84(21)**: 4316-4318 (2004).

[21] Koo J., Kleinstreuer C., Impact Analysis of Nanoparticle Motion Mechanisms on the Thermal Conductivity of Nanofluids, *Int. Commun. Heat Mass Transfer*, **32(9)**: 1111-1118 (2005).

[22] Evans W., Fish J., Keblinski P., Role of Brownian Motion Hydrodynamics on Nanofluid Thermal Conductivity, *Appl. Phys. Lett.*, **88(9)**: 93-116 (2006).

[23] Nie C., Marlow W., Hassan Y., Discussion of Proposed Mechanisms of Thermal Conductivity Enhancement in Nanofluids, *Int. J. Heat Mass Transfer*, **51(5)**: 1342-1348 (2008).

[24] Yu W., Choi S.U.S., The Role of Interfacial Layers in the Enhanced Thermal Conductivity of Nano-Fluids: A Renovated Maxwell Model, *J. of Nanoparticles Res.*, **5(1–2)**: 167-171 (2003).

[25] Leong K., Yang C., Murshed S., A Model for the Thermal Conductivity of Nanofluids–the Effect of Interfacial Layer, *J. of Nanoparticles Res.*, **8(2)**: 245-254 (2006).

[26] Putnam S.A., Cahill D.G., Ash B.J., Schadler L.S., High-Precision Thermal Conductivity Measurements as a Probe of Polymer/Nanoparticle Interfaces, *J. Appl. Phys.*, **94(10)**: 6785-6788 (2003).

[27] Evans W., Prasher R., Fish J., Meakin P., Phelan P., Keblinski P., Effect of Aggregation and Interfacial Thermal Resistance on Thermal Conductivity of Nanocomposites and Colloidal Nanofluids, *Int. J. Heat Mass Transfer*, **51(5)**: 1431-1438 (2008).

[28] Prasher R., Phelan P.E., Bhattacharya P., Effect of Aggregation Kinetics on the Thermal Conductivity Of Nanoscale Colloidal Solutions (Nanofluid), *Nano Letters*, **6(7)**: 1529-1534 (2006).

[29] Zhu H., Zhang C., Liu S., Tang Y., Yin Y., Effects of Nanoparticle Clustering and Alignment on Thermal Conductivities of Fe_3O_4 Aqueous Nanofluids, *Appl. Phys. Lett.*, **89(2)**: 023123 (2006).

[30] Kakac S., Pramuanjaroenkij A., Single Phase and Two Phase Treatments of Convective Heat Transfer Enhancement with Nanofluids–A State–of–the–Art Review *Int. J. Therm. Sci.*, **100**: 75-97 (2016).

[31] Buongiorno J., Convective Transport in Nanofluids, *J. Heat Transfer*, **128(3)**: 240-250 (2006).

[32] Ding Y., Wen D., Particle Migration in a Flow of Nanoparticle Suspensions, *Powder Technology*, **149(2-3)**: 84-92 (2005).

[33] Malvandi A., Heysiattalab S., Ganji D.D., Thermophoresis and Brownian Motion Effects on Heat Transfer Enhancement at Film Boiling of Nanofluids over a Vertical Cylinder, *J. Mol. Liq.*, **216**: 503-509 (2016).

[34] Eastman J.A., Phillpot S.R., Choi S.U.S., Keblinski P., Thermal Transport in Nanofluids, *Annual Reviews in Material Res.*, **34**: 219-246 (2004).

[35] Singh P., Gupta R., Wanchoo R.K., Experimental Investigation of Forced Convection of Glycol – Based CuO Nanofluids Flowing Through Straight Tubes and Helical Coils, *J. Nanofluids*, **6(2)**: 220-231 (2016).

[36] Singh P., Gupta R., Wanchoo R.K., Forced Convective Heat Transfer Studies on Glycol Based Al_2O_3 Nanofluids Flowing Through Straight Tubes and Helical Coils. *J. Nanofluids*, **7(1)**: 37-51 (2017).

[37] Singh P., Sharma P., Gupta R., Wanchoo R.K. Heat Transfer Characteristics of Propylene Glycol/Water Based Magnesium Oxide Nanofluid Flowing through Straight Tubes and Helical Coils, *Journal of Thermal Engineering*, **4(1)**: 1737-1755 (2018).

[38] Sharma K.V., L Syam S., Laminar Convective Heat Transfer and Friction Factor of Al_2O_3 Nanofluid in Circular Tube Fitted with Twisted Tape Inserts, *International Journal of Automotive and Mechanical Engineering (IJAME)*, **3**: 265-278 (2011).

[39] Sharma P., Singh P., Gupta R., Wanchoo R.K., Hydrodynamic Studies on MgO Nanofluid Flowing Through Straight Tubes and Coils, *J. Nanofluids*, **6(3)**: 558-566 (2017a).

[40] Raei B., Ghadi A., Bozorgian A., Heat Integration of Heat Exchangers Network Using Pinch Technology, in: 19th International Congress of Chemical and Process Engineering CHISA, (2010).

[41] Pourabadeh A., Nasrollahzadeh B., Razavi R., Bozorgian A., Najafi M., A.Oxidation of FO and N_2 Molecules on the Surfaces of Metal-Adopted Boron Nitride Nanostructures as Efficient Catalysts, *J. Struct. Chem.*, **59**: 1484–1491 (2018).

[42] Esmaeili Bidhendi M., Asadi Z., Bozorgian A., et al., New magnetic Co3O4/Fe3O4 Doped Polyaniline Nanocomposite for the Effective and Rapid Removal of Nitrate Ions from Ground Water Samples, *Environ. Prog. Sustainable Energy*, **39**: e13306 (2019).

[43] Bozorgian A., Arab Aboosadi Z., Mohammadi A., Honarvar B., Azimi A., Optimization of Determination of CO2 Gas Hydrates Surface Tension in the Presence of Non-Ionic Surfactants and TBAC, *Eurasian Chem. Commun.*, **2**: 420-426 (2020).

[44] Mashhadizadeh J., Bozorgian A., Azimi A., Investigation of the Kinetics of Formation of Clatrit-like dual hydrates TBAC in the Presence of CTAB, *Eurasian Chem. Commun.*, **2**: 536-547 (2020).

[45] Norouzi N., Bozorgian A., Dehghani M., Best Option of Investment in Renewable Energy: A Multicriteria Decision-Making Analysis for Iranian Energy Industry, *Journal of Environmental Assessment Policy and Management*, 22: No. 01n02, 2250001 (2020).

[46] Norouzi N., Ebadi A., Bozorgian A., Hoseyni S.J., Vessally E., Energy and Exergy Analysis of Internal Combustion Engine Performance of Spark Ignition for Gasoline, Methane, and Hydrogen Fuels, *Iran. J. Chem. Chem. Eng. (IJCCE)*, **40**: 1909-1930 (2021).

[47] Bozorgian A., Arab Aboosadi Z., Mohammadi A., Honarvar B., Azimi A., Statistical Analysis of the Effects of Aluminum Oxide (Al_2O_3) Nanoparticle, TBAC, and APG on Storage Capacity of CO_2 Hydrate Formation, *Iran. J. Chem. Chem. Eng. (IJCCE)*, **41**: 220-231 (2022).

[48] Ahmadpour A., Bozorgian A., Eslamimanesh A., Mohammadi A.H., Photocatalytic Treatment of Spontaneous Effluent of Petrochemical Effluents by TiO2 CTAB Synthetic Nanoparticles, *Desalin. Water Treat.*, **249**: 297-308 (2022).

[49] Norouzi N., Ebadi A., Bozorgian A., Hoseyni S.J., Vessally E., Cogeneration System of Power, Cooling, and Hydrogen from Geothermal Energy: An Exergy Approach, *Iran. J. Chem. Chem. Eng. (IJCCE)*, **41**: 706-721 (2022).

[50] Bozorgian A., Arab Aboosadi Z., Mohammadi A., Honarvar B., Azimi A., Determination of CO2 Gas Hydrates Surface Tension in the Presence of Nonionic Surfactants and TBAC, *Rev. Roum. Chim.*, **65**: 1061-1065 (2020).

[51] Kanani M., Kanani N., Batooie N., Bozorgian A., Barghi A., Rezania Sh., Removal of Rhodamine 6G dye using one-pot Synthesis of Magnetic Manganese Graphene Oxide: Optimization by Response Surface Methodology, *Environ. Nanotechnol., Monit. Manage.*, **18**: 100709 (2022).

[52] Norouzi N., 4E Analysis and Design of a Combined Cycle with a Geothermal Condensing System in Iranian Moghan Diesel Power Plant, *International Journal of Air-Conditioning and Refrigeration*, **28(03)**: 2050022 (2020).

[53] Norouzi N., 4E analysis of a fuel cell and gas turbine hybrid energy system, *Biointerface Res. Appl. Chem.*, **11**: 7568-7579 ( ).